J|A|C|S ARTICLES

Published on Web 12/16/2010

Sub-40 nm Zeolite Suspensions via Disassembly of Three-Dimensionally Ordered Mesoporous-Imprinted Silicalite-1

Pyung-Soo Lee,[†] Xueyi Zhang,[†] Jared A. Stoeger,[†] Abdulla Malek,[‡] Wei Fan,[†] Sandeep Kumar,[†] Won Cheol Yoo,[§] Saleh Al Hashimi,[‡] R. Lee Penn,[§] Andreas Stein,[§] and Michael Tsapatsis*,[†]

Department of Chemical Engineering and Materials Science, University of Minnesota, Minneapolis, Minnesota 55455, United States, Chemical Engineering Program, The Petroleum Institute, Abu Dhabi, United Arab Emirates, and Department of Chemistry, University of Minnesota, Minneapolis, Minnesota 55455, United States

Received September 3, 2010; E-mail: tsapatsis@umn.edu

Abstract: Zeolite nanocrystals were prepared from three-dimensionally ordered mesoporous-imprinted (3DOm-i) silicalite-1 by a fragmentation method involving sonication and dissolution within a certain pH range. 3DOm-i silicalite-1 with spherical elements with diameters ranging from 10 to 40 nm and a wide range of crystal sizes (100−200 nm, 500−600 nm, and 1−2 μm) was used as the starting material. The highest yield (57%) of isolated nanocrystals was obtained for 3DOm-i silicalite-1 with a crystal size of 100−200 nm and a spherical element diameter of 40 nm. The smallest nanocrystals obtained, albeit in very low yields, had a 10 nm diameter. Preparation of stable silicalite-1 nanocrystal suspensions fragmented from 20 and 40 nm 3DOm-i silicalite-1 was demonstrated. Cryogenic transmission electron microscopy showed that the isolated zeolite nanocrystals can be used as seeds for the epitaxial growth of silicalite-1. An application of these findings was demonstrated: silicalite-1 nanocrystal suspensions were used to deposit seed layers on porous α-alumina disks, which were converted to continuous thin (300−400 nm) films by secondary growth that exhibited both high permeances and separation factors (3.5×10^{-7} mol m^{-2} s^{-1} Pa^{-1} and 94−120, respectively, at 150 °C) for *p*- and *o*-xylene.

Introduction

Secondary growth from a zeolite seed layer[1,2] is an established method for the fabrication of zeolite films and membranes.[3−5] The size, shape, and spatial arrangement of seed crystals as well as their evolution during secondary growth determine the preferred orientation, grain and grain boundary size, and other microstructural characteristics that affect mechanical and transport properties and consequently determine the performance of zeolite membranes.[6−12]

Zeolite seed layers are normally formed on substrates of interest from zeolite powders and suspensions by a variety of wet and dry deposition methods.[13−17] Dispersible zeolite nanoparticles with diameters of <50 nm are desirable for the formation of thin and densely populated seed layers that, upon secondary growth, can lead to well-intergrown, thin zeolite films. Such films are highly desirable as separation membranes on the basis of the expectation that they may combine high selectivity with previously unrealized high fluxes. Other emerging zeolite film applications, including low-*k* dielectrics[18−20] and nanocomposite membranes,[21,22] could also benefit from the availability of such suspensions. Moreover, zeolite suspensions

[†] Department of Chemical Engineering and Materials Science, University of Minnesota.
[‡] The Petroleum Institute.
[§] Department of Chemistry, University of Minnesota.

(1) Lovallo, M. C.; Tsapatsis, M. *AIChE J.* **1996**, *42*, 3020–3029.
(2) Valtchev, V.; Schoeman, B. J.; Hedlund, J.; Mintova, S.; Sterte, J. *Zeolites* **1996**, *17*, 408–415.
(3) Snyder, M. A.; Tsapatsis, M. *Angew. Chem., Int. Ed.* **2007**, *46*, 7560–7573.
(4) Caro, J.; Noack, M. *Microporous Mesoporous Mater.* **2008**, *115*, 215–233.
(5) Tsapatsis, M.; Gavalas, G. R. *MRS Bull.* **1999**, *24*, 30–35.
(6) Lai, Z. P.; Bonilla, G.; Diaz, I.; Nery, J. G.; Sujaoti, K.; Amat, M. A.; Kokkoli, E.; Terasaki, O.; Thompson, R. W.; Tsapatsis, M.; Vlachos, D. G. *Science* **2003**, *300*, 456–460.
(7) Choi, J.; Ghosh, S.; Lai, Z. P.; Tsapatsis, M. *Angew. Chem., Int. Ed.* **2006**, *45*, 1154–1158.
(8) Jeong, H. K.; Krohn, J.; Sujaoti, K.; Tsapatsis, M. *J. Am. Chem. Soc.* **2002**, *124*, 12966–12968.
(9) Choi, J.; Ghosh, S.; King, L.; Tsapatsis, M. *Adsorption* **2006**, *12*, 339–360.
(10) Lee, I.; Buday, J. L.; Jeong, H. K. *Microporous Mesoporous Mater.* **2009**, *122*, 288–293.
(11) Liu, Y.; Li, Y. S.; Yang, W. S. *J. Am. Chem. Soc.* **2010**, *132*, 1768–1769.
(12) Coronas, J. *Chem. Eng. J.* **2010**, *156*, 236–242.
(13) Yoon, K. B. *Acc. Chem. Res.* **2007**, *40*, 29–40.
(14) Lee, J. S.; Lee, Y. J.; Tae, E. L.; Park, Y. S.; Yoon, K. B. *Science* **2003**, *301*, 818–821.
(15) Lee, J. S.; Kim, J. H.; Lee, Y. J.; Jeong, N. C.; Yoon, K. B. *Angew. Chem., Int. Ed.* **2007**, *46*, 3087–3090.
(16) Matsukata, M.; Ogura, M.; Osaki, T.; Rao, P.; Nomura, M.; Kikuchi, E. *Top. Catal.* **1999**, *9*, 77–92.
(17) Lee, J. A.; Meng, L. L.; Norris, D. J.; Scriven, L. E.; Tsapatsis, M. *Langmuir* **2006**, *22*, 5217–5219.
(18) Li, Z. J.; Lew, C. M.; Li, S.; Medina, D. I.; Yan, Y. S. *J. Phys. Chem. B* **2005**, *109*, 8652–8658.
(19) Volksen, W.; Miller, R. D.; Dubois, G. *Chem. Rev.* **2010**, *110*, 56–110.

may be of interest for drug delivery[23] and imaging applications. Although zeolite nanoparticles with diameters of <50 nm have been reported for several frameworks (SOD,[24,25] FAU,[26,27] MFI,[28−32] and MEL[18]), dispersible zeolite nanoparticles for coating applications are rather difficult to prepare. Most approaches rely on the control of nucleation and growth, which is hampered because of our insufficient understanding of silica speciation and interactions in these complex mixtures. An alternative approach to generating zeolite nanoparticles is disassembly or dissolution of appropriately structured zeolite crystals.[33,34]

Three-dimensionally ordered mesoporous-imprinted (3DOm-i) silicalite-1 is a type of hierarchical zeolite that is composed of uniform nanoscale zeolitic spherical elements with their size determined by the 3DOm template employed during synthesis. The spherical elements have a cubic close-packed (ccp) arrangement and are interconnected through their 12 nearest neighbors, forming single crystals composed of many oriented and interconnected spherical elements, as shown in Figure 1.[34] 3DOm-i silicalite-1 has both the micropores of the MFI framework zeolite (with sizes similar to those of many industrially important molecules[35]) and ordered mesopores corresponding to the tetrahedral and octahedral interstitial spaces of a close-packed lattice of spherical elements. Considering their open structure, their monodisperse and tunable spherical elements with sizes of <50 nm, and the symmetrically positioned connections between the 3DOm-i spherical elements, disassembly of 3DOm-i particles can be a promising method for producing uniform, isolated MFI nanoparticles. In ref 34, we reported that isolated spherical elements were obtained by fragmentation using a short sonication treatment (5 min). This conclusion was based on transmission electron microscopy (TEM) observations, and the yield was not determined.

In this paper, we report the preparation of sub-40 nm crystals via the fragmentation of 3DOm-i silicalite-1 by sonication within a certain pH range. 3DOm-i silicalite-1 crystals with varying crystal sizes and spherical element sizes have been used to determine the yield of zeolite nanocrystals by the fragmentation method. Secondary growth of the nanocrystals was demonstrated using cryogenic transmission electron microscopy (cryo-TEM) and implemented for fabricating well-intergrown, ultrathin silicalite-1 films. A combination of rapid thermal processing (RTP) and conventional calcination techniques was used to remove the structure-directing agents (SDAs) from the zeolite films.[36] The resulting zeolite membranes were thin (<400 nm) and exhibited an attractive combination of high flux and separation factor for xylene isomers.

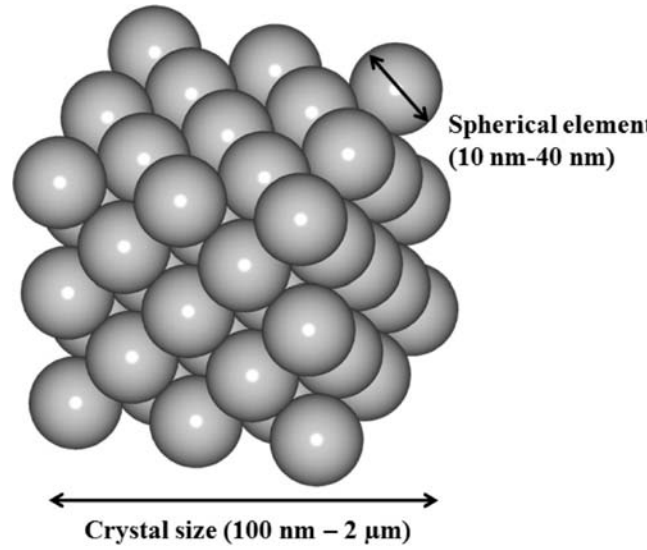

Figure 1. Conceptual schematic of a 3DOm-i silicalite-1 single crystal indicating the range of spherical element and crystal sizes achieved. As a result of the confined crystal growth in 3DOm carbon, the spherical elements are interconnected and uniformly oriented forming a single 3DOm-i crystal.

Experimental Section

Syntheses of Size-Tunable Silica Nanoparticles, 3DOm Carbon, and 3DOm-i Silicalite-1. Silica nanoparticle sols were synthesized by hydrolysis of tetraethyl orthosilicate (TEOS, 98%, Aldrich) with aqueous solutions of basic amino acid lysine (Sigma-Aldrich) as described in previous reports.[34,37,38] Steam-assisted crystallization (SAC) was used for the confined synthesis of 3DOm-i silicalite-1 in the 3DOm carbon template.[34,39] The synthesis sol was a 9:0.15:50:390:180 $TPA_2O/Na_2O/SiO_2$/water/ethanol mixture for all samples. The SAC was conducted at three different temperature−time combinations: 85 °C for 5 days, 135 °C for 3 days, and 180 °C for 2 days.

Fragmentation of 3DOm-i Silicalite-1. (1) Dialysis Method for Studying the Effect of pH. Dissolution of 3DOm-i silicalite-1 was performed in a dialysis tube (Spectra/Por 3, Spectrum Laboratories Inc.), which allowed separation of silicalite-1 crystals from dissolved silicate and other ions. A polypropylene beaker was filled with 1 L of deionized water (Millipore Elix, 10 MΩ cm). A tetrapropylammonium hydroxide solution (TPAOH, 1.0 M in water, Sigma-Aldrich) or L-lysine (Sigma-Aldrich) was added to the beaker to achieve the desired initial pH value for dissolution; 75.0 mg of

(20) Li, Z. J.; Johnson, M. C.; Sun, M. W.; Ryan, E. T.; Earl, D. J.; Maichen, W.; Martin, J. I.; Li, S.; Lew, C. M.; Wang, J.; Deem, M. W.; Davis, M. E.; Yan, Y. S. *Angew. Chem., Int. Ed.* **2006**, *45*, 6329–6332.
(21) Perez, E. V.; Balkus, K. J.; Ferraris, J. P.; Musselman, I. H. *J. Membr. Sci.* **2009**, *328*, 165–173.
(22) Bae, T. H.; Liu, J. Q.; Lee, J. S.; Koros, W. J.; Jones, C. W.; Nair, S. *J. Am. Chem. Soc.* **2009**, *131*, 14662–14663.
(23) Vallet-Regi, M.; Ramila, A.; del Real, R. P.; Perez-Pariente, J. *Chem. Mater.* **2001**, *13*, 308–311.
(24) Schoeman, B. J.; Sterte, J.; Otterstedt, J. E. *Zeolites* **1994**, *14*, 208–216.
(25) Fan, W.; Morozumi, K.; Kimura, R.; Yokoi, T.; Okubo, T. *Langmuir* **2008**, *24*, 6952–6958.
(26) Mintova, S.; Olson, N. H.; Bein, T. *Angew. Chem., Int. Ed.* **1999**, *38*, 3201–3204.
(27) Holmberg, B. A.; Wang, H. T.; Norbeck, J. M.; Yan, Y. S. *Microporous Mesoporous Mater.* **2003**, *59*, 13–28.
(28) Motuzas, J.; Julbe, A.; Noble, R. D.; Guizard, C.; Beresnevicius, Z. J.; Cot, D. *Microporous Mesoporous Mater.* **2005**, *80*, 73–83.
(29) Valtchev, V. P.; Faust, A. C.; Lezervant, J. *Microporous Mesoporous Mater.* **2004**, *68*, 91–95.
(30) Van Grieken, R.; Sotelo, J. L.; Menendez, J. M.; Melero, J. A. *Microporous Mesoporous Mater.* **2000**, *39*, 135–147.
(31) Song, W.; Justice, R. E.; Jones, C. A.; Grassian, V. H.; Larsen, S. C. *Langmuir* **2004**, *20*, 8301–8306.
(32) Aguado, J.; Serrano, D. P.; Escola, J. M.; Rodriguez, J. M. *Microporous Mesoporous Mater.* **2004**, *75*, 41–49.
(33) Stein, A.; Li, F.; Wang, Z. *J. Mater. Chem.* **2009**, *19*, 2094–2098.
(34) Fan, W.; Snyder, M. A.; Kumar, S.; Lee, P. S.; Yoo, W. C.; McCormick, A. V.; Penn, R. L.; Stein, A.; Tsapatsis, M. *Nat. Mater.* **2008**, *7*, 984–991.
(35) Kokotailo, G. T.; Lawton, S. L.; Olson, D. H.; Meier, W. M. *Nature* **1978**, *272*, 437–438.
(36) Choi, J.; Jeong, H. K.; Snyder, M. A.; Stoeger, J. A.; Masel, R. I.; Tsapatsis, M. *Science* **2009**, *325*, 590–593.
(37) Snyder, M. A.; Lee, J. A.; Davis, T. M.; Scriven, L. E.; Tsapatsis, M. *Langmuir* **2007**, *23*, 9924–9928.
(38) Yokoi, T.; Sakamoto, Y.; Terasaki, O.; Kubota, Y.; Okubo, T.; Tatsumi, T. *J. Am. Chem. Soc.* **2006**, *128*, 13664–13665.
(39) Schmidt, I.; Madsen, C.; Jacobsen, C. J. H. *Inorg. Chem.* **2000**, *39*, 2279–2283.

3DOm-i silicalite-1 powder was transferred to a centrifuge tube containing 8 mL of the same solution as in the beaker, to which sonication for approximately 5 min was applied to ensure the crystals were separated from each other before dissolution. The mixture was then transferred to a rinsed dialysis tube, which was then sealed and placed in the beaker. The solution in the beaker was stirred slowly, allowing the dialysis tube to rotate. The pH of the solution in the beaker was monitored regularly. The solution outside the dialysis tube was changed regularly to a fresh one with the desired initial pH, to keep the pH within the desired range and remove silicate species produced by dissolution. After the dissolution had been conducted for the desired time, the solution outside the dialysis tube was changed to deionized water, to remove the silicate species. After 1 day, the sol inside the dialysis tube was collected and dried at 70 and 135 °C.

(2) Sonication Method for Higher-Yield Fragmentation of 3DOm-i Silicalite-1. Ultrasonication was used to fragment 3DOm-i silicalite-1 for further characterization and subsequent deposition onto a porous support for membrane growth. First, 0.1 g of 3DOm-i silicalite-1 was added to 20 mL of deionized water in conical tubes. The 3DOm-i silicalite-1 suspensions were then sonicated (Bransonic model 5510R-DTH) for 90 min, after which ice was added to the sonicator water bath to lower the temperature to 15 °C. The water bath temperature was maintained in a range from 15 to 30 °C during sonication. The period of sonication cycles totaled 18 h for a typical run, but times of up to 60 h were investigated. The sols were unbuffered, and the pH ranged from 10 (at the beginning) to 9 (at the end) during the fragmentation process. After the sonication, centrifugation at 11000*g* relative centrifugal force (RCF) for 10 min was performed to separate the clear sol supernatant containing silicalite-1 nanocrystals from the larger partially fragmented particles. The nanocrystal suspensions were dried at 95 °C for 5 h and then dried at 180 °C for 1 day. To calculate yields, the final weights of the dried powders were measured.

Cryo-TEM Study of Secondary Growth of Isolated Spherical Elements. The silicalite-1 seeds used to study secondary growth were 40 nm spherical elements isolated from 3DOm-i silicalite-1 crystals using the sonication procedure described above. After isolation, the seeds were suspended in water at a concentration of 1 mg of silicalite-1/mL. The suspension was visually stable with no precipitation at room temperature for a period of at least 3 months. The growth sols used for this study were prepared as described by Davis et al.[40] with the following compositions: 5:9:8100:20 SiO_2/TPAOH/H_2O/EtOH (denoted as C1), 10:9:8100:40 SiO_2/TPAOH/H_2O/EtOH (denoted as C2), and 20:9:8100:80 SiO_2/TPAOH/H_2O/EtOH (denoted as C3).

The 1 mg/mL seed suspension was mixed with an appropriate volume of growth sol to yield suspensions that were 0.2 mg of silicalite-1/mL with compositions consistent with C1, C2, or C3. The suspension was sealed in a centrifuge tube with Teflon tape to prevent evaporation of the solvent and was heated in a convection oven at 70 °C. After a certain time, the centrifuge tube was removed and plunged into an ice bath (0 °C). A cryo-TEM sample was prepared from the suspension immediately afterward.

Cryo-TEM sample preparation was conducted in an FEI Vitrobot Mark III vitrification robot.[41] A droplet of the suspension was placed onto a carbon/Formvar-coated copper grid (Ted Pella Inc.) in the climate chamber of the Vitrobot system, where the temperature was kept at 25 °C and the relative humidity was kept at 100%. The specimen was transferred under liquid nitrogen to a Gatan 626 DH cryo-transfer specimen holder.

Fabrication of the Zeolite Membrane. Homemade porous α-alumina disks were used as supports for silicalite-1 membrane growth.[9] We have employed a masking technique as introduced by Hedlund and co-authors.[42] A viscous solution of polyvinyl alcohol (PVA, 80% hydrolyzed, Aldrich) was prepared by dissolving 12.5 g of PVA in 10 g of deionized water at 70 °C. First, the solution was spread over the top surface of the alumina support using a spatula and dried for 12 h at room temperature. Next, paraffin wax (melting point of 70−80 °C, Aldrich) was used to fill the pores of the alumina disk by vacuum infiltration (20 in. Hg) at 90 °C for 1 h. Excess wax remaining on the surface of the alumina disk after the 1 h period was removed with a tissue before the wax solidified. Then, PVA on the alumina surface was removed in tap water (refreshed every 4 h) at 50 °C for 12 h, exposing the alumina surface while leaving the pores filled with wax. After the PVA had been removed, 300 μL of a zeolite nanocrystal suspension (0.5 wt %) was dropped onto the surface of the alumina disk and dried for 5 h at room temperature. Excess silicalite-1 nanocrystals on the support surface were leveled off by rubbing on weighting paper (VWR Scientific Products, 4 in. × 4 in.). The support was calcined at 550 °C for 8 h in flowing air. This treatment should be sufficient for removal of the wax according to previous reports from Hedlund and co-authors.[42,43] Secondary growth was conducted by placing the seeded alumina disk vertically in a Teflon linear with composition C3 at 90 °C for 11 h. Rapid thermal processing (RTP, nominal heating to 700 °C within 1 min, no hold time, and rapid cooling to room temperature) and subsequent conventional calcination (1 °C/min to 500 °C, held for 2 h) were conducted to remove the occluded SDA molecules using the setup reported previously.[36] In contrast to the previously reported RTP method for the calcination of thick zeolite membranes, no holding time at the maximum temperature was applied.

Characterization. Scanning electron microscopy (SEM) images were collected on Hitachi S-900 and Hitach S-4700 instruments after the samples were coated with 1 nm of Pt. The samples for TEM studies were prepared via application of a few droplets of the sol onto a copper grid coated with a holey carbon film (Ted Pella Inc.). The grid was then allowed to air-dry. Imaging was performed at −177 °C on an FEI Tecnai G^2 F30 transmission electron microscope operating at 300 kV. All TEM images were captured using a CCD camera. Small-angle X-ray diffraction (SAXD) measurements were taken on a homemade pinhole SAXD line with a sample-to-detector distance of 100 cm using Cu Kα radiation. N_2 adsorption and desorption isotherms were measured at 77 K on a Quantachrome Autosorb-1 system. Conventional *t*-plot methods were used for extracting micropore properties. X-ray diffraction (XRD) patterns were acquired using a PANalytical X-Pert PRO MPD X-ray diffractometer equipped with a Co source and a Bruker AXS D5005 diffractometer with a Cu source. A ζ potential analyzer (ZetaPALS, Brookhaven Instruments Corp.) was used for dynamic light scattering (DLS) measurements. Particle sizes were calculated using software provided by Brookhaven Instruments Corp.

Permeation Measurements. The xylene isomer vapor permeation experiments were conducted in Wicke-Kallenbach mode with a stainless steel permeation cell fitted inside a Thermolyne 48000 furnace, using an equimolar *p*-xylene/*o*-xylene feed as previously reported.[9] For the equimolar feed used here, the separation factor is defined as the ratio of the molar fluxes.

Results and Discussion

Terminology. Figure 1 shows what is meant herein by the crystal size and spherical element of 3DOm-i silicalite-1. For the sake of simplicity, we use the diameter of the amorphous

(40) Davis, T. M.; Drews, T. O.; Ramanan, H.; He, C.; Dong, J. S.; Schnablegger, H.; Katsoulakis, M. A.; Kokkoli, E.; McCormick, A. V.; Penn, R. L.; Tsapatsis, M. *Nat. Mater.* **2006**, *5*, 400–408.
(41) Iancu, C. V.; Tivol, W. F.; Schooler, J. B.; Dias, D. P.; Henderson, G. P.; Murphy, G. E.; Wright, E. R.; Li, Z.; Yu, Z. H.; Briegel, A.; Gan, L.; He, Y. N.; Jensen, G. J. *Nat. Protoc.* **2006**, *1*, 2813–2819.
(42) Hedlund, J.; Sterte, J.; Anthonis, M.; Bons, A. J.; Carstensen, B.; Corcoran, N.; Cox, D.; Deckman, H.; De Gijnst, W.; de Moor, P. P.; Lai, F.; McHenry, J.; Mortier, W.; Reinoso, J. *Microporous Mesoporous Mater.* **2002**, *52*, 179–189.
(43) Hedlund, J.; Jareman, F.; Bons, A. J.; Anthonis, M. *J. Membr. Sci.* **2003**, *222*, 163–179.

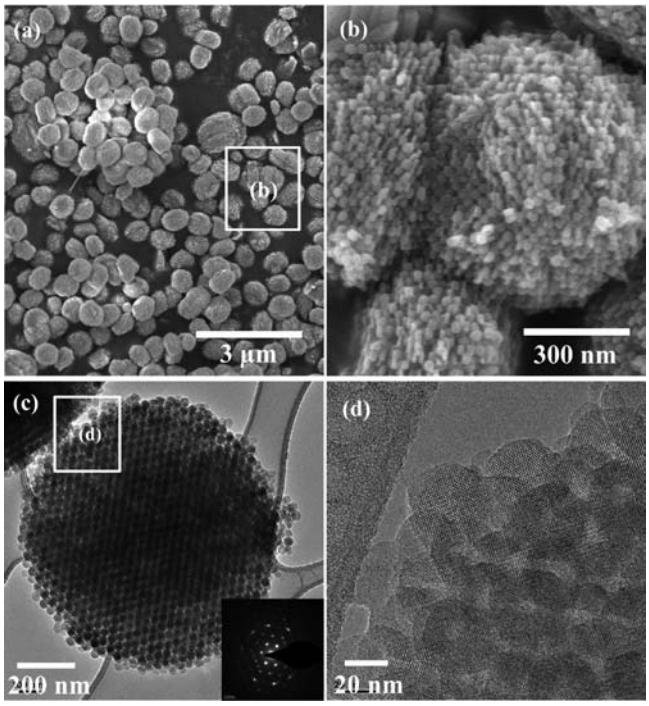

Figure 2. (a and b) SEM and (c and d) TEM images of 40 nm 3DOm-i silicalite-1. The inset in panel c is the selected area electron diffraction (SAED) pattern of the crystal ([010] zone axis).

lysine−silica spherical nanoparticles to refer to the cage size of 3DOm carbons and the size of spherical elements in the 3DOm-i zeolites produced. The crystal sizes refer to the sizes of the imprinted crystal particles and were varied from 100 nm to 2 μm, and the spherical elements were tuned from 10 to 40 nm.

(1) Synthesis of 3DOm-i Silicalite-1 with Tunable Spherical Element and Crystal Size. 3DOm-i silicalite-1 can be synthesized inside the ordered spherical cages of a 3DOm carbon template by steam-assisted crystallization (SAC).[34,39] By controlling the diameter of the lysine−silica spheres used to form the 3DOm carbon, we can control the corresponding diameters of the spherical elements from 10 to 50 nm.[34] Figure 2 shows SEM and TEM images of 3DOm-i silicalite-1 samples prepared in 3DOm carbon with a 40 nm cage size by SAC at 135 °C for 3 days. The low-magnification view in Figure 2a reveals an average crystal size of approximately 1 μm. In the higher-magnification image shown in Figure 2b, the spherical elements forming the 3DOm-i silicalite-1 are visible. The TEM image in Figure 2c reveals an ordered arrangement of spherical elements and mesopores, while the electron diffraction pattern in the inset of Figure 2c and the higher-magnification image in Figure 2d confirm that the entire particle comprised of 40 nm spherical elements is a single silicalite-1 crystal. Panels a−d of Figure S1 of the Supporting Information are the corresponding SEM and TEM images of 20 nm 3DOm-i silicalite-1 prepared using the same conditions described above.

In addition to 3DOm-i silicalite-1, a few faceted zeolites (e.g., indicated by the arrow in Figure S1a of the Supporting Information) formed outside the 3DOm carbon template; 95% of the silicalite-1 crystals were crystallized inside the 3DOm carbon as determined by counting the number of 3DOm-i silicalite-1 particles and faceted zeolites from such SEM images. Figure 3 shows SEM images of 30 nm 3DOm-i silicalite-1. SAC was conducted at 85 °C for 5 days to crystallize the zeolite particles seen in Figure 3a, while those in panels b and c of Figure 3 were obtained after 3 days at 135 °C and after 2 days at 180 °C, respectively. The chemical composition remained the same for the three cases (9:0.15:50:390:180 TPA_2O:Na_2O:

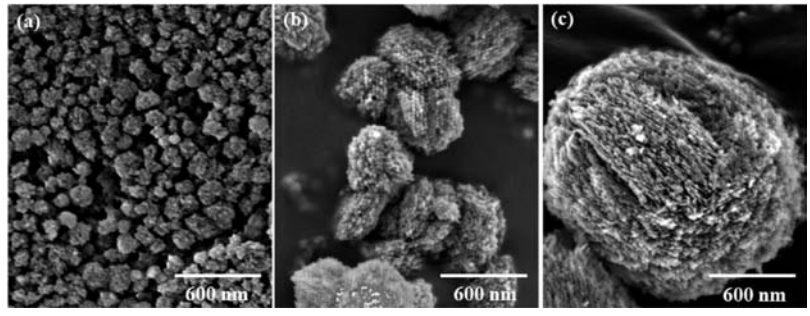

Figure 3. SEM images of 30 nm 3DOm-i silicalite-1 with crystal sizes of (a) 100−200 nm, (b) 500−600 nm, and (c) 1 μm.

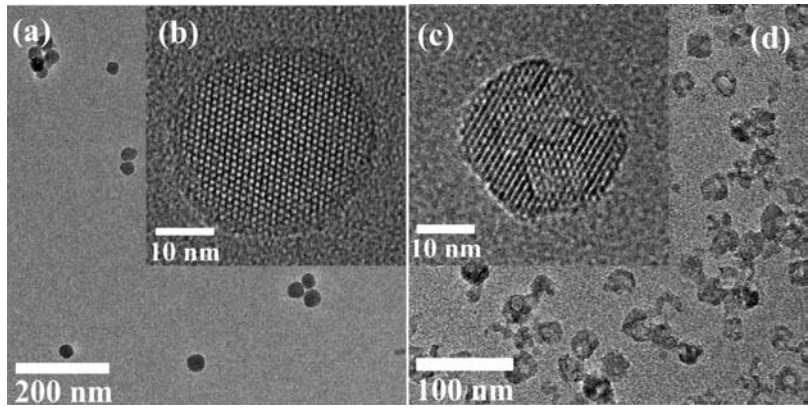

Figure 4. TEM images of silicalite-1 nanocrystals obtained after the dialysis dissolution procedure with 40 nm 3DOm-i silicalite-1 over different pH ranges for 7 days: (a and b) pH 9.0−10.0 and (c and d) pH 11.0−12.0.

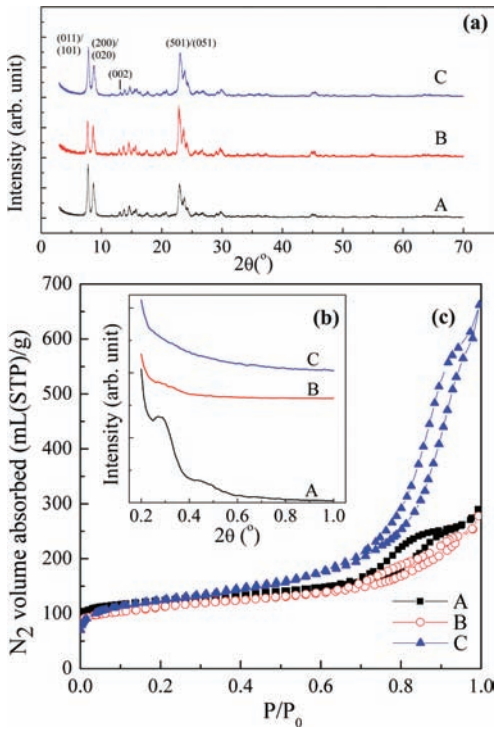

Figure 5. (a) Wide and (b) small-angle X-ray diffraction (Cu Kα radiation, $\lambda = 1.542$ Å) patterns, along with (c) N_2 adsorption isotherms of 40 nm 3DOm-i silicalite-1 before and after dialysis dissolution treatment. Trace A: as-synthesized. Traces B and C: after treatment at pH 9.0−10.0 and 11.0−12.0, respectively, for 7 days.

SiO_2:water:ethanol). Although the spherical element sizes of the 30 nm 3DOm-i silicalite-1 shown in Figure 3 are the same, their crystal sizes varied (100−200 nm, 500−600 nm, and 1 μm in panels a−c of Figure 3, respectively), indicating that control of the 3DOm-i silicalite-1 crystal sizes may be achieved by altering the reaction time and temperature.

(2) Disassembly of 3DOm-i Silicalite-1 To Yield Isolated Spherical Elements as Single Nanocrystals. Although the spherical elements in 3DOm-i silicalite-1 are connected in a close-packed arrangement, the connections are relatively thin sections (few nanometers) so that they could be separated by dissolution and/or a disturbance such as ultrasonication. In a certain pH range, isolation of the individual spherical elements from 3DOm-i crystals can be achieved, while in a different pH range, silicalite-1 nanocrystals with a "fractured egg-shell" morphology were formed. On the basis of these observations, we developed an additive-free dissolution procedure for preparing zeolite seeds in considerable yield.

Table 1. Yields of Zeolite Nanocrystals with Respect to 3DOm-i Silicalite-1 (grams of nanocrystals per gram of 3DOm-i silicalite-1) after Sonication of Nine Different 3DOm-i Samples with the Indicated Crystal and Spherical Element Sizes[a]

	20 nm element size	30 nm element size	40 nm element size
100−200 nm crystals	4 ± 1%	18 ± 2%	57 ± 3%
500−600 nm crystals	<4%	6 ± 1%	10 ± 1%
1−2 μm crystals	4 ± 1%	9 ± 1%	15 ± 1%

[a] For an explanation of the terms 3DOm-i crystal and spherical element size, see the schematic in Figure 1.

(2.1) Effect of Dissolution pH. Figure 4 shows morphologies of products obtained from 40 nm 3DOm-i silicalite-1 using the dialysis dissolution procedure and two different pH ranges. For dialysis dissolution at pH 9.0−10.0, intact spherical elements can be obtained, as shown in panels a and b of Figure 4. For dialysis dissolution at pH 11.0−12.0, two types of objects are obtained: isolated spherical elements with observable mesopores (Figure 4c,d) and smaller silicalite-1 nanocrystal fragments having irregular shapes. The etched morphology shown in Figure 4c is attributed to dissolution. Figure S2 of the Supporting Information shows that similar conclusions can be drawn when using 3DOm-i silicalite-1 with 25 nm spherical elements.

Although the etched morphology obtained over the higher pH range (pH 11.0−12.0) does not appear to be appropriate for the formation of ordered seed layers, the nanoscopic fragments obtained (a sampling of small fragments is shown in Figure S3 of the Supporting Information) are fundamentally significant because they demonstrate that zeolite nanoparticles that contain only a few unit cells exist and can be stable with respect to structural transformation, aggregation, or electron beam damage.

The XRD patterns of the silicalite-1 crystals show little change after the dialysis dissolution procedure (Figure 5a), indicating that the spherical objects shown in Figure 4 have the MFI framework in both pH ranges. As expected, because of the disassembly of the 3DOm-i crystals to individual spherical elements, SAXD measurements (Figure 5b) show that dialysis dissolution treatment under both conditions nearly eliminated the ccp order. After treatment, the specific micropore volume, as measured using N_2 adsorption, of the particles decreased for both pH ranges (from 0.129 to 0.089 mL/g). As seen in the isotherms of Figure 5c, dialysis dissolution treatment between pH 9.0 and 10.0 led to a mesopore distribution that was wider than that of 3DOm-i crystals, which can be attributed to the loss of the packing order of isolated spherical elements. Using pH 11.0−12.0 resulted in a greatly increased total pore volume from the new mesopores formed within the isolated crystals.

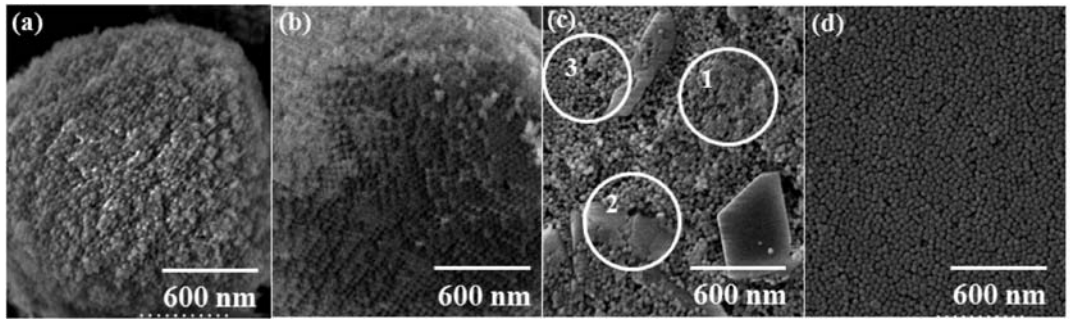

Figure 6. SEM images of 40 nm 3DOm-i silicalite-1 before (a) and after sonication for (b) 4 and (c) 18 h at pH 9−10. The different regions marked 1−3 in panel c correspond to intact 3DOm-i silicalite-1, silicalite-1 grown outside the 3DOm carbon, and silicalite-1 nanocrystals, respectively. (d) SEM image of silicalite-1 nanocrystals present in the supernatant after centrifugation of the suspension obtained after sonication for 18 h.

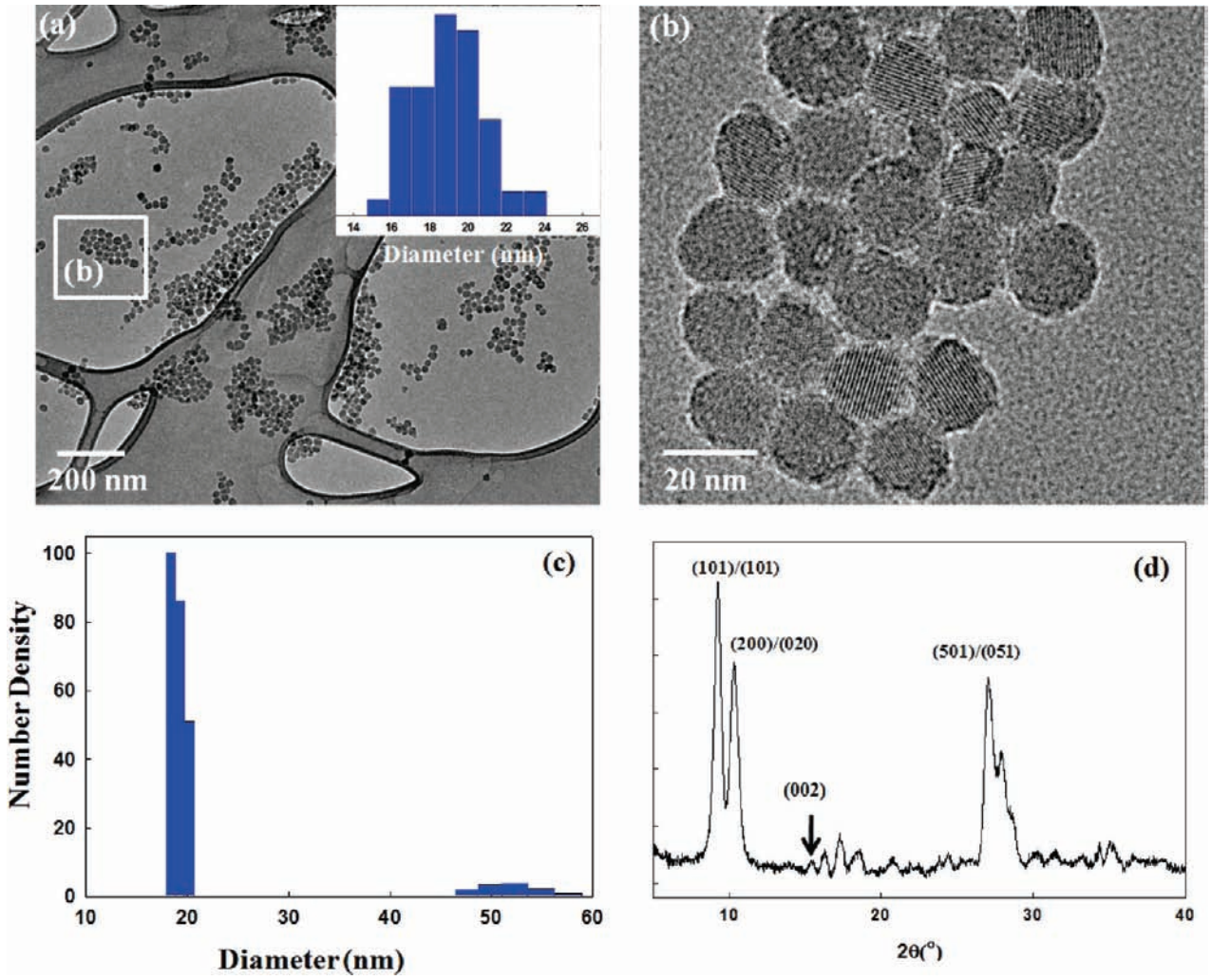

Figure 7. Characterization of silicalite-1 nanocrystal suspensions obtained after sonication of 20 nm 3DOm-i silicalite-1 and purification by centrifugation: (a) low-magnification TEM, (b) high-magnification TEM, (c) DLS, and (d) wide-angle X-ray diffraction (Co Kα radiation, $\lambda = 1.790$ Å). The inset of panel a shows the TEM particle size distribution.

(2.2) Dissolution by Sonication of Unbuffered Sols. The dialysis dissolution procedure described above requires pH adjustment, and therefore, it is not an ideal candidate for scale-up. An alternative process that requires no additives was developed on the basis of two observations: (1) Unbuffered silicalite-1 suspensions exhibit basic pH, and (2) silicalite-1 dissolution releases silicic acid species, which reduces the initial basic pH. The alternative process is simply sonication of the 3DOm-i silicalite-1 aqueous sol at the sol concentration ranges described in the Experimental Section. Under these conditions, the pH is kept between 9 and 10 with no need for pH adjustment.

Figure 6 shows a series of SEM images of 1−2 μm crystals of 40 nm 3DOm-i silicate-1 before and after the sonication treatment. Comparing panels a and b of Figure 6 reveals that the opal-like ccp appearance of the 3DOm-i crystals becomes more pronounced after sonication for 4 h. This is probably caused by the removal of loosely packed spherical elements present on their outer surfaces. After sonication for 18 h (Figure 6c), considerable fragmentation is observed. In Figure 6c, region 1, outlined in white, is indicative of unbroken 3DOm-i silicalite-1. Region 2 is indicative of faceted zeolite particles grown outside of the 3DOm carbon template. Region 3, which comprises the majority of the observable area, shows isolated zeolite nanocrystals. As the sonication time increased beyond 18 h, the pH of 3DOm-i silicalite-1 suspensions decreased below 9, causing observable precipitation. Thus, considering nanozeolite yield, the sonication time for fragmentation was set to 18 h.

As discussed above, an aqueous 3DOm-i silicalite-1 suspension obtained after the sonication treatment consists of unbroken 3DOm-i silicalite-1, faceted zeolite crystals formed outside of 3DOm carbon, and the desirable isolated silicalite-1 nanocrystals (Figure 6c). Because of the size difference between the latter and the other two components, they can be separated by centrifugation. The SEM image in Figure 6d shows silicalite-1 nanocrystals present in the supernatant obtained by centrifugation at 11000*g* RCF for 10 min.

By variation of crystal sizes and spherical elements, 12 3DOm-i silicalite-1 samples were prepared for fragmentation using the sonication procedure. Different pore sizes of 3DOm carbon from 10 to 40 nm were used, and 3DOm-i silicalite-1 crystal sizes of 100−200 nm, 500−600 nm, and 1−2 μm were selected. Table 1 shows the yield of silicalite-1 nanocrystals with respect to the starting amount of 3DOm-i silicalite-1 crystals. Although intact isolated crystals obtained from 10 nm 3DOm-i silicalite-1 can be observed by TEM (Figure S4 of the Supporting Information), the yield was too small to determine. Silicalite-1 nanocrystal suspensions can be obtained with appreciable yield (≥4%) as the sizes of the spherical elements

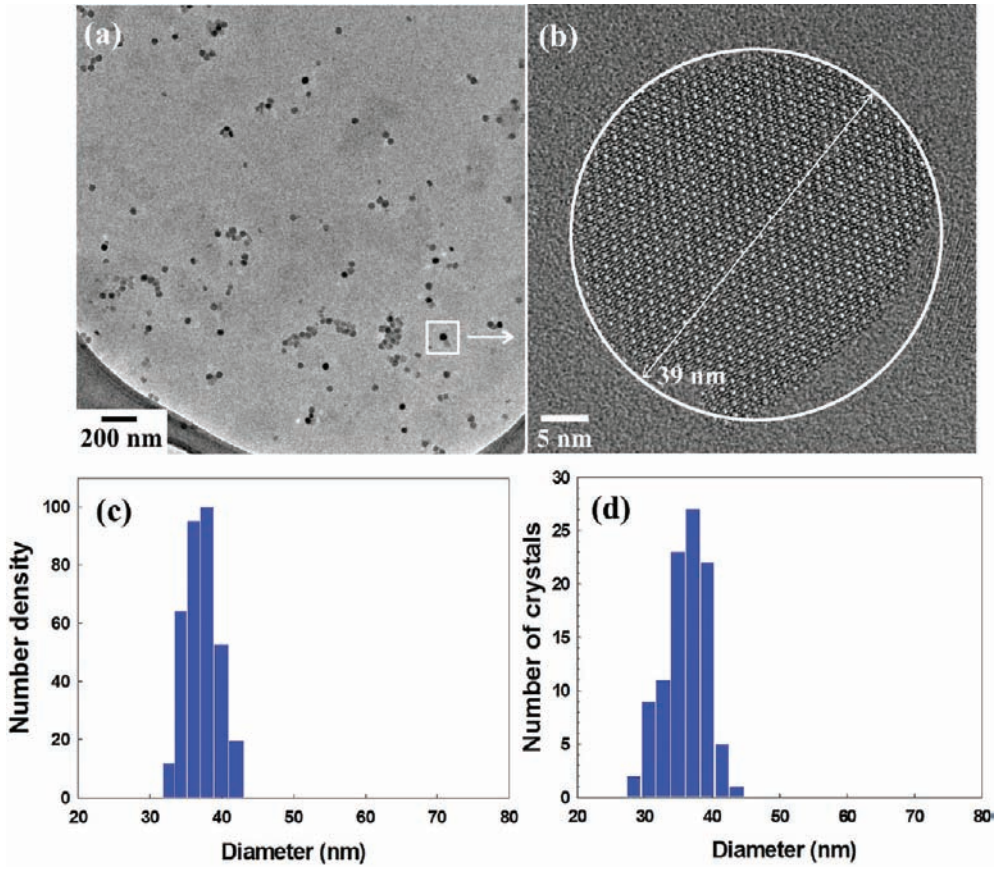

Figure 8. Characterization of silicalite-1 suspensions obtained after sonication of 40 nm 3DOm-i silicalite-1 and purification by centrifugation: (a) low-magnification TEM and (b) high-magnification TEM images. Particle size distribution from DLS (c) and from TEM images (d). Because the silicalite-1 nanoparticles are not perfect spheres, the diameter of a circle approximating the TEM projection was used for determining the TEM particle size distribution shown in panel d. For example, the particle shown in panel b ([010] zone axis) was approximated with a circle 39 nm in diameter.

become larger than 20 nm. Two observations can be made. (1) A higher yield was obtained from 3DOm-i silicalite-1 having larger spherical elements. (2) The crystal size of 3DOm-i silicalite-1 affects the yield of nanocrystals. More specifically, 100−200 nm crystals exhibited higher yields than 500−600 nm and 1−2 μm crystals. However, the trend with crystal size is not monotonic.

Figure 7 shows characterization data of isolated zeolite nanocrystals fragmented from 20 nm 3DOm-i silicalite-1. Figure 7a is a low-magnification TEM image of silicalite-1 nanocrystals isolated by the sonication procedure. The inset shows the particle size distribution determined from this image (Figure 7a). Because the particles are not perfect spheres, their size was approximated by the diameter of a circle enclosing them. A high-magnification TEM image in Figure 7b shows the crystalline nature of the isolated zeolite nanocrystals. The DLS data from suspensions shown in Figure 7c also reveal the presence of ~20 nm nanocrystals with a small fraction of 50 nm crystals (possibly small clusters of spherical elements). To further explore the crystallinity of the zeolite nanocrystals, the sol was dried on a silicon wafer for XRD. Figure 7d shows peaks consistent with the silicalite-1 crystal structure. Figure 8 shows the corresponding data from nanocrystals fragmented from 40 nm 3DOm-i silicalite-1 crystals.

Figures 7 and 8 show that starting from aqueous suspensions of spherical 20 and 40 nm lysine−silica particles, we can obtain zeolite nanoparticles that are approximately spherical with a narrow particle size distribution centered a few nanometers below the size expected from a perfect replication. Figure 9a summarizes the steps from lysine−silica nanoparticles to zeolite nanocrystals, i.e., (i) synthesis of silica nanoparticles, (ii) formation of colloidal crystals by assembly and calcination of the silica nanoparticles, (iii) synthesis of the 3DOm carbon, and (iv) confined synthesis of 3DOm-i zeolite in carbon followed by (v) calcination and (vi) fragmentation of 3DOm-i zeolite crystals to zeolite nanoparticles. In step (ii), because of sintering at the particle−particle interfaces, the nearest neighbor center-to-center distances of the colloidal crystals are smaller than the starting particle size prepared in step (i). Even assuming perfect replication in steps (iii) and (v), we expect a further reduction in size as well as shape deviation from perfect spheres to be introduced during confined growth step (iv) (e.g., by imperfect filling of cages because of faceting and diffusion limitations) and fragmentation step (vi) (e.g., because of dissolution and imperfect breaking at connections) as schematically shown in Figure 9a. To further illustrate the deviations observed from perfect replication of the shape and size of the starting amorphous colloidal silica particles to the final crystalline zeolite nanoparticles, we show, in Figure 9b, three high-resolution images of zeolite crystals obtained starting from 40 nm silica particles, all imaged down the *b* axis. The dotted lines indicate approximate circles that encompass the particles, while the bold circles show the expected shapes of the projection from perfect replication of the 40 nm amorphous silica starting particles.

(3) Cryo-TEM Study of the Secondary Growth on the Silicalite-1 Spherical Elements. Cryo-TEM images in Figure 10 show the evolution of silicalite-1 nanocrystals from 40 nm 3DOm-i silicalite-1 in a sol with composition C3 (see the Experimental

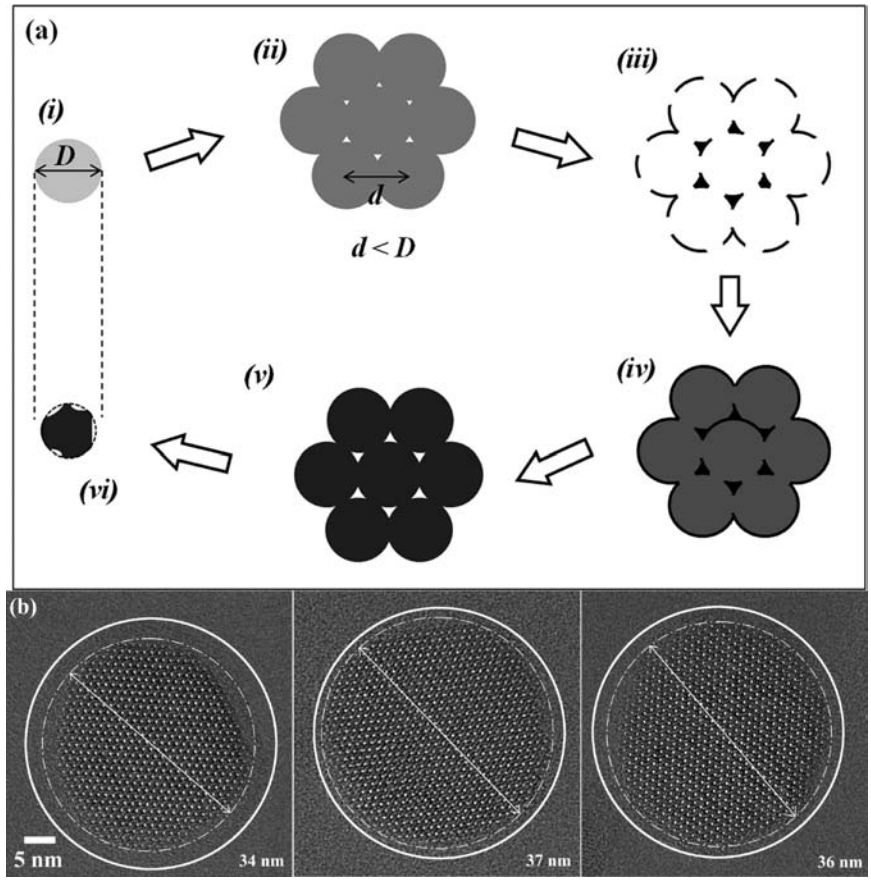

Figure 9. Change in size and shape of spherical elements during preparation of silicalite-1 nanocrystals. (a) Schematic of preparation steps of silicalite-1 nanocrystals starting from lysine−silica nanoparticles. (b) TEM images of silicalite-1 nanocrystals. The diameter of bold circles represents 40 nm, and the dotted lines indicate approximate circles that encompass the particles.

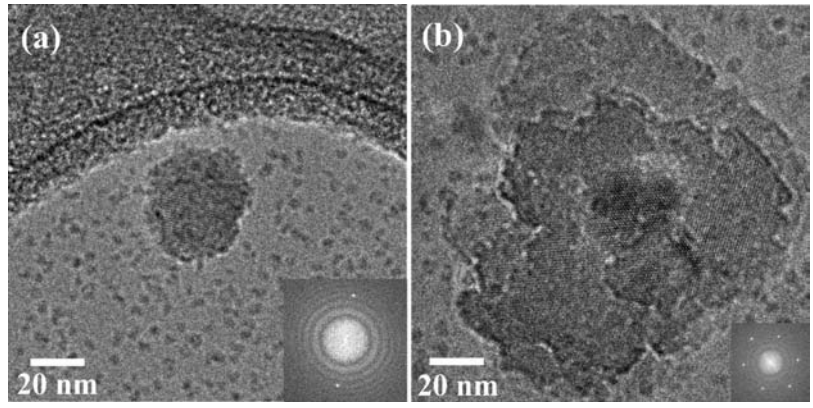

Figure 10. Representative cryo-TEM images of silicalite-1 nancrystals fragmented from 40 nm 3DOm-i silicalite-1 heated at 70 °C in a C3 sol for (a) 6 h [the inset is the FFT of the image of the particle showing spots ($d = 1$ nm) consistent with (200) or (020) planes from MFI structure] and (b) 36 h (the inset is the FFT of the entire image of the particle showing consistence with MFI structure throughout indexed as the [100] or [010] zone axis).

Section) at 70 °C over a period of 36 h. C3 sols have a silica concentration above the solubility limit and are known to contain ~5 nm amorphous silica nanoparticles.[40,44] Previous studies have shown that silicalite-1 seed crystals in C3 sols can grow by secondary growth.[45] In a C3 sol, the added silicalite-1 nanocrystals are present among a high concentration of such 5 nm nanoparticles. After 6 h, the seeds showed no obvious growth, as seen in Figure 10a. However, the surfaces of the seed particles appear rougher, which might be attributed to dissolution in the basic growth sol and/or attachment of the 5 nm nanoparticles onto the seeds. After 12, 18, and 24 h (Figure S5 of the Supporting Information), there is clear evidence of growth. As time proceeds, the seed particles continue to grow to 142 ± 15 nm, as seen in Figure 10b. Throughout the growth process, the grown parts appeared fully crystalline, and the crystallographic orientations of the seed and the grown parts were identical.

Secondary growth of the seeds was also attempted using C1 and C2 sols. The SiO_2 concentration in C1 is below, that in C2

(44) Rimer, J. D.; Lobo, R. F.; Vlachos, D. G. *Langmuir* **2005**, *21*, 8960–8971.
(45) Nikolakis, V.; Kokkoli, E.; Tirrell, M.; Tsapatsis, M.; Vlachos, D. G. *Chem. Mater.* **2000**, *12*, 845–853.

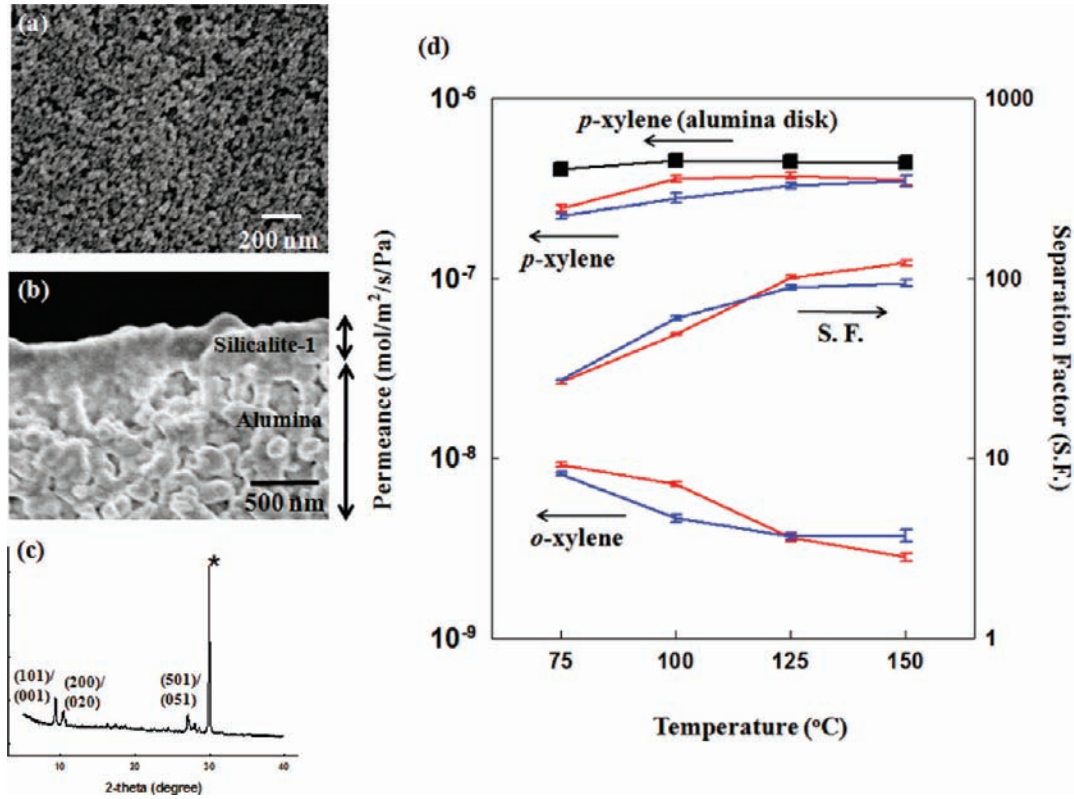

Figure 11. Seeded growth of zeolite membranes: (a) SEM image of the seed layer on an α-alumina disk support, (b) cross-sectional image, and (c) wide-angle X-ray diffraction (Co Kα radiation, $\lambda = 1.790$ Å) of a zeolite membrane. An asterisk denotes the peak from the alumina disk. (d) *p*-Xylene and *o*-xylene permeances and corresponding separation factors of two zeolite membranes indicated by red and blue colors. Error bars represent the standard deviation from the mean. SEM (a and b) and wide-angle X-ray diffraction (c) were conducted with the membrane with permeation properties indicated in red. The permeance of *p*-xylene nearly matches that observed through the support (■).

near, and that in C3 above the silica solubility limit. As expected, dissolution was observed and the seed size was reduced to 34 ± 3 nm after exposure to the C1 solution at 70 °C for 36 h (Figure S6a of the Supporting Information). Similar treatment in C2 sols resulted in a size increase to approximately 56 ± 5 nm (Figures S6b and S7 of the Supporting Information). The TEM images reveal lattice fringes extending throughout the particles grown in C3 (see Figure 10 and Figure S5 of the Supporting Information) and a 5−15 nm thick layer without any fringes at the periphery of those grown in C2 (Figure S6b of the Supporting Information). A defocus series taken in the cryo-transmission electron microscope (Figure S7 of the Supporting Information) shows no evidence of crystalline order in this outer layer. On the basis of these observations, we selected composition C3 to perform secondary growth for membrane fabrication.

(4) Fabrication of Silicalite-1 Membranes by Secondary Growth. Zeolite nanocrystals made by the fragmentation of 3DOm-i silicalite-1 were used as seed crystals to fabricate zeolite membranes following the approach of Hedlund and co-authors.[42] Figure 11a is a representative SEM image of a seeded layer of zeolite nanocrystals deposited on the surface of the alumina disk. After calcination, the entire support surface was seeded. The SEM image in Figure 11b shows a cross-sectional view of a zeolite membrane after secondary growth for 11 h and the removal of SDAs with the procedure described in the Experimental Section. A well-intergrown zeolite membrane with a thickness in the 300−400 nm range is shown, while the silicalite-1 crystal structure is clearly shown by the XRD data of Figure 11c. Because of the thin zeolite layer, the α-alumina peak from the substrate has a much higher intensity compared to those of the peaks corresponding to the randomly oriented silicalite-1 film.

Figure 11d shows *p*-/*o*-xylene isomer permeation data from two similarly prepared membranes. High separation factors were obtained at 125 °C (90−100) and 150 °C (94−120), indicating high-quality silicalite-1 membranes.[6,36,46,47] High permeance was achieved because of the submicrometer thickness of the membrane. Permeances at 150 °C were $\geq 3.5 \times 10^{-7}$ mol m^{-2} s^{-1} Pa^{-1}. These permeances are significantly higher compared to those reported in ref 36 for thick c-oriented MFI membranes. Considering that the limiting flux from the bare alumina disk is ca. 4.0×10^{-7} mol m^{-2} s^{-1} Pa^{-1}, it appears that further improvements to the flux will require different support materials.

The performance of membranes reported here is similar to that of membranes with similar microstructure prepared using seed layers made by rubbing of larger polycrystalline brittle seeds.[47] Although further research is needed with regard to the engineering of wet versus dry coating, the current wet approach is compatible with dip coating technology used for membrane manufacturing, and therefore, it could be more readily applicable for zeolite membrane fabrication. Moreover, the nanocrystals reported here may also find uses in the formation of nanocomposites,[21,22] spin-on low-*k* films,[18−20] and possibly other applications like drug delivery[23] and imaging after adsorption of appropriate components. To the best of our knowledge,

(46) Xomeritakis, G.; Lai, Z. P.; Tsapatsis, M. *Ind. Eng. Chem. Res.* **2001**, *40*, 544–552.
(47) Yoo, W. C.; Stoeger, J. A.; Lee, P.-S.; Tsapatsis, M.; Stein, A. *Angew. Chem., Int. Ed.* **2010**, *49*, 8699–8703.

silicalite-1 suspensions with size-tunable, spherical, twin-free particles smaller than 40 nm cannot be produced otherwise. Extension of this hierarchical nanomanufacturing approach to other zeolite structure types and compositions is underway and will be reported elsewhere.

Conclusions

The spherical element sizes of 3DOm-i silicalite-1 can be controlled by choosing different cage sizes of 3DOm carbon from 10 to 40 nm. Via variation of temperature and time of steam-assisted crystallization, the crystal size of 3DOm-i silicalite-1 may also be tuned from 100 nm to 1−2 μm. Suspensions of spherical zeolite nanocrystals in the range of 10−40 nm were prepared by the fragmentation of 3DOm-i silicalite-1 using ultrasonication at pH 9−10 and subsequent centrifugation. The highest yield was obtained from a parent 3DOm-i silicalite-1 with 40 nm spherical elements and a crystal size of 100−200 nm after sonication for 18 h. Appreciable yields were obtained for spherical element sizes down to 20 nm. Although isolated 10 nm crystals were observed, the yields were too small to be determined. One of their possible uses was demonstrated by coating porous α-alumina disks to form densely packed zeolite layers. Because of the uniformity of the deposited seed layers, a relatively short secondary growth time (11 h) and a low temperature (90 °C) were sufficient conditions for the formation of well-intergrown zeolite films. The resulting zeolite membranes were very thin (in the range of 300−400 nm), and high fluxes (limited by the support resistance for the fast permeating component) with a high separation factor (94−120 at 150 °C) were measured for *p*- and *o*-xylene.

Acknowledgment. We gratefully acknowledge financial support from the Petroleum Institute of Abu Dhabi through the ADMIRE (Abu Dhabi-Minnesota Institute for Research Excellence) partnership and from the National Science Foundation (NSF-NIRT CMMI 0707610). Portions of this work were conducted at the University of Minnesota, Institute of Technology Characterization Facility, which receives partial support from the National Science Foundation through the NNIN program.

Supporting Information Available: Additional SEM and TEM images. This material is available free of charge via the Internet at http://pubs.acs.org.

JA107942N